

FRB Periodicity: Mild Pulsars in Tight O/B-star Binaries

Maxim Lyutikov¹, Maxim V. Barkov^{1,2}, and Dimitrios Giannios¹
Department of Physics, Purdue University, 525 Northwestern Avenue, West Lafayette, IN 47907-2036, USA

² Astrophysical Big Bang Laboratory, RIKEN, 2-1 Hirosawa, Wako, Saitama 351-0198, Japan

*Received 2020 March 30; revised 2020 April 4; accepted 2020 April 8; published 2020 April 22

Abstract

Periodicities observed in two fast radio burst (FRB) sources (16 days in FRB 180916.J0158+65 and 160 days in FRB 121102) are consistent with that of tight, stellar-mass binary systems. In the case of FRB 180916.J0158+65 the primary is an early OB-type star with the mass-loss rate $\dot{M} \sim 10^{-8}$ – $10^{-7}M_{\odot}$ yr⁻¹, and the secondary is a neutron star. The observed periodicity is not intrinsic to the FRB's source, but is due to the orbital phase-dependent modulation of the absorption conditions in the massive star's wind. The observed relatively narrow FRB activity window implies that the primary's wind dynamically dominates that of the pulsar, $\eta = L_{\rm sd}/(\dot{M}v_wc) \leqslant 1$, where $L_{\rm sd}$ is the pulsar spin-down, \dot{M} is the primary's wind mass-loss rate, and v_w is its velocity. The condition $\eta \leqslant 1$ requires a mildly powerful pulsar with $L_{\rm sd} \lesssim 10^{37}\,{\rm erg\,s^{-1}}$. The observations are consistent with magnetically powered radio emission originating in the magnetospheres of young, strongly magnetized neutron stars, the classical magnetars.

Unified Astronomy Thesaurus concepts: Magnetars (992); Stellar winds (1636); Radio transient sources (2008); Close binary stars (254)

1. FRB Periodicity due to the Orbital Motion in the O/B-NS Binary

1.1. Observations and Outline of the Model

The CHIME collaboration announced a P=16 day periodicity from FRB 180916.J0158+65 (The CHIME/FRB Collaboration et al. 2020). Analysis to date from the 76 m Lovell telescope on the original repeater FRB 121102 also indicated a periodicity of $P\sim160$ days (Rajwade et al. 2020). These are important observations that shed light on the origin of FRBs, as we discuss in the present Letter. Below we concentrate on the case of FRB 180916.J0158+65.

The observed periodicity is most likely due to the orbital motion of a binary system. (In the Appendix we discuss an unlikely periodicity due to geodetic precession in an extremely tight binary. Free precession models were also proposed Levin et al. 2020; Zanazzi & Lai 2020.)

The orbital semimajor axis for the case of FRB 180916. J0158+65 evaluates to

$$P = 2\pi \sqrt{\frac{a^3}{GM_{\odot}(m_{\rm PSR} + m_{\rm MS})}}$$

$$a = 4 \times 10^{12} m_{\rm tot, 1}^{1/3} P_{1.2}^{2/3} \text{ cm}, \qquad (1)$$

where $m_{\rm PSR}$ is (the presumed) neutron star's mass and $m_{\rm MS}$ is the primary's mass in solar masses and $m_{\rm tot} = (m_{\rm PSR} + m_{\rm MS})$. (We refer to the the O/B star as "a primary," while to the neutron star as a "companion.") In this Letter we use the notation $Ax = A/10^x$, $m_{\rm tot}$ is measured in solar masses M_{\odot} , and P is in days.

Both the pulsar, loci of the FRB, and the primary produce winds: a relativistic wind by the pulsar and wind with velocity $v_w \sim \text{few } 10^3 \text{ km s}^{-1}$ by a main-sequence star (Vink et al. 2001). We hypothesize that the observed periodicity is due to absorption of the FRB pulses in the primary's wind; see Figure 1.

The interacting pulsar's and the primary's winds create a conically shaped cavity around the less powerful source. The primary's winds can be highly optically thick at radio waves due to free—free absorption, while the relativistic pulsar wind is, basically, transparent to radio waves. A transparent cone-like zone is, therefore, created behind the pulsar, modified into spiral structure by the orbital motion.

The radio waves propagating within this spiral structure do not experience free–free absorption. After they enter the primary's wind, at a larger distance, the wind's density and the corresponding absorption coefficient are substantially reduced. Thus, the dynamics of interacting winds creates transparency windows when the observer sees the pulsar through the spiral structure (Bosch-Ramon & Barkov 2011; Bosch-Ramon et al. 2012, 2015).

Since the active window is observed to be less than 50% of the orbital period, the primary's wind should dominate over that of the pulsar. This requires that the momentum parameter η is less than unity,

$$\eta = \frac{L_{\rm sd}}{\dot{M}v_{\rm w}c} \leqslant 1. \tag{2}$$

(This regime is opposite to the case of Black Widow-type pulsar binaries; Fruchter et al. 1988.)

The typical opening of the transparency wedge behind a pulsar as seen in simulations of Bosch-Ramon et al. (2015) is $\sim\!15^\circ\!-\!20^\circ;$ this is weakly dependent on the momentum parameter as long as $\eta\lesssim0.3.$ This is consistent with the active phase observed in FRB 180916.J0158+65.

Simulations of Bosch-Ramon et al. (2015), see also Figure 1, demonstrate that the wind cavity can extend out to 10–30 times the binary separation radius. As a result, the cavity created by the pulsar's wind can reduce the absorption optical depth by a factor as large as 10^3 : if at the location of the pulsar the primary's wind is still moderately, $\tau \leq 10^3$, optically thick to infinity, and the observer's line of sight lies close to the equatorial plane, within $\sim 15^\circ - 20^\circ$, then the source turns transparent to radio emission for part of the orbit.

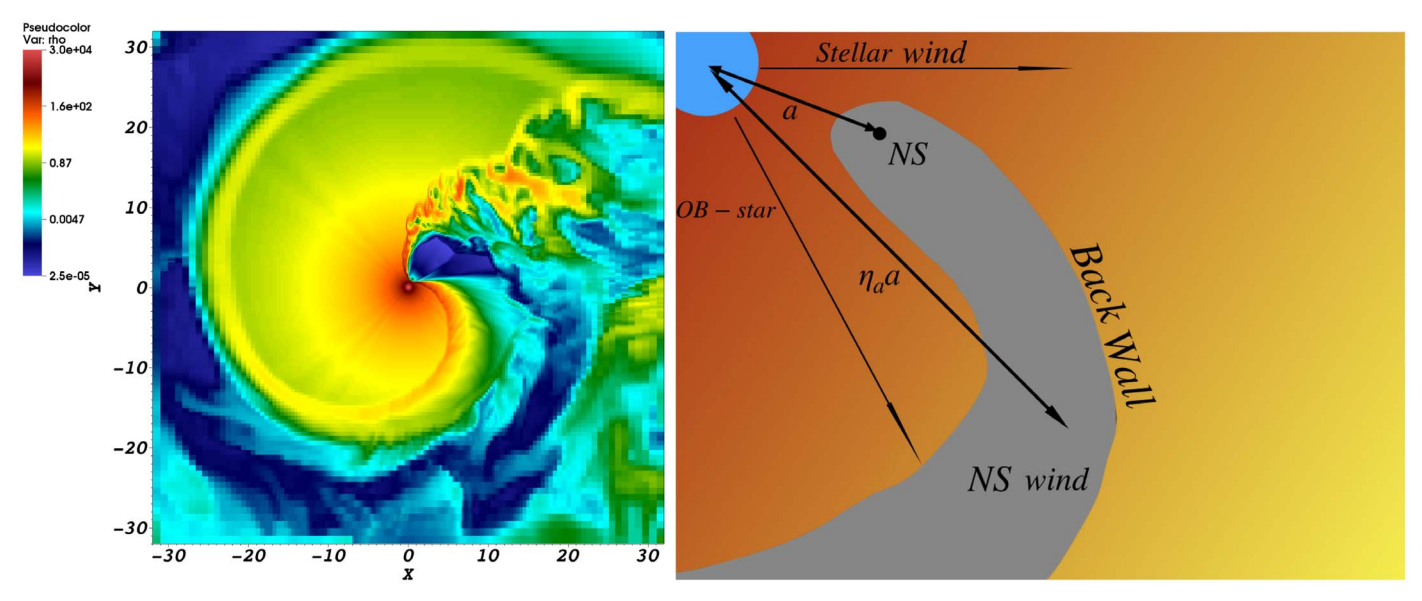


Figure 1. Left panel: reprocessed simulations of Bosch-Ramon et al. (2015) of interacting winds of the B star and pulsar. Right panel: artistic image of the interacting winds. The pulsar wind creates a narrow low-density cavity that extends to distances much larger than the orbital separation by a factor $\eta_a \sim 10$ –30. At that point the density of the primary's wind is lower by η_a^2 and the absorption coefficient is reduced by η_a^4 and the optical depth by η_a^3 .

1.2. Free-Free Absorption in the Primary's Wind

Below we make the numerical estimates of the proposed model. We parameterize the location of the "back wall" of the cavity as $\eta_a a$ (a is orbital separation), and normalize the numerical estimates to $\eta_a=10^{1.5}\eta_{a,1.5}.$ The free–free optical depth forming the location of the "back

The free-free optical depth forming the location of the "back wall" of the cavity to infinity should be of the order of unity for radio waves to escape. Using the free-free-absorption coefficient $\kappa_{\rm ff}$ (Lang 1999), assuming temperature $T=10^4$ K, and scaling the "back wall" radius with the orbital separation (1), we find

$$\begin{split} \kappa_{\rm ff} &= 3.28 \times 10^{-7} T_4^{-1.35} \nu_{\rm 1GHz}^{-2.1} \frac{\rm EM}{\rm pc} \\ \dot{M} &= 4\pi n m_p (\eta_a a)^2 v_w \\ \tau_{\rm ff} &\sim 5 \times 10^{-3} \, \eta_{a,1.5}^{-3} \dot{M}_{-7.5}^2 T_4^{-1.35} \nu_{\rm 1GHz}^{-2.1} m_{\rm tot,1} v_{w,8.5}^{-2}, \end{split} \tag{3}$$

here EM = $\int_a^\infty n^2 dr$ is the emission measure. So, a mass-loss rate of $\dot{M} \sim 3 \times 10^{-8} M_{\odot} \, \mathrm{yr}^{-1}$ can give substantial optical depth to free-free absorption for a source at distance a, but transparent conditions when the source is observed through the "back wall" of a cavity that extends to $\sim 30a$.

Using the mass-loss rate \dot{M} from (3) and requiring the primary's momentum dominance in the wind-wind interaction, we estimate the pulsar spin-down luminosity:

$$L_{\rm sd} \leqslant 5 \times 10^{36} \eta_{-0.5} \dot{M}_{-7.5} v_{w,8.5} \, {\rm erg \ s^{-1}}.$$
 (4)

Thus, the pulsar can produce mildly strong winds.

The model limits the mass-loss rate of the main-sequence star both from below (the wind-wind interaction should be dominated by the main-sequence star), and from above (too powerful winds are optically thick to free-free absorption out to very large distances). Early B-type stars and late O-type stars fit the required mass-loss range. Late B-type stars have insufficiently strong winds, while earlier O-type stars remain optically thick to large distances (Vink et al. 2001; Krticka 2014).

1.3. Nonlinear Propagation Effects

Strong radio waves can affect nonlinearly the free-free absorption coefficient in the wind (Lu & Phinney 2019). Qualitatively, a strong electromagnetic wave in weakly magnetized plasma induces an electron's oscillations with the momentum

$$p_{\perp} \sim a_0 m_e c$$

$$a_0 = \frac{eE}{m_e c \omega},$$
(5)

where a_0 is the laser intensity parameter and E is the electric field in the wave (Akhiezer et al. 1975). If the quiver energy $\sim a_0^2 m_e c^2$ is larger than the temperature, $a_0 \geqslant \sqrt{T/(m_e c^2)}$, then the motion of the electrons is determined by the wave itself, not the temperature.

For typical parameters of FRB 180916.J0158+65 (The CHIME/FRB Collaboration et al. 2020; total fluence F = 10 Jy ms, duration $\tau = 2$ ms, and distance $d_{\text{FRB}} = 150$ Mpc) the luminosity and the total energy in a single burst evaluate to

$$L_{\rm FRB} = 4\pi \frac{d_{\rm FRB}^2 F}{\tau} = 3 \times 10^{40} \, {\rm erg \ s^{-1}},$$
 (6)
 $E_{\rm FRB} = 4\pi d_{\rm FRB}^2 F = 6 \times 10^{37} \, {\rm erg}.$

The nonlinearity parameter is then

$$a_0 = \frac{e\sqrt{F}}{am_e c^{3/2} \sqrt{\tau} \,\omega} \approx 1. \tag{7}$$

Thus, the FRB can heat the plasma to relativistic energies! As a result, a sufficiently strong pulse can propagate much further than expected from the linear theory, heating up the plasma and decreasing the absorption. But the radio pulse does not have enough energy to escape, as we discuss next.

As the particles are heated by the wave, the plasma absorption coefficient $\kappa_{\rm ff}$ decreases, allowing a wave to propagate further. The total amount of the material the FRB

heats is

$$M_h \sim \frac{m_p E_{\text{FRB}}}{a_0^2 m_e c^2} = 10^{20} \,\text{g}.$$
 (8)

This huge amount of material heated to relativistic electron temperatures is still much smaller than contained in the wind within the orbit

$$M_w \approx \frac{a}{v_{vi}} \dot{M} = 3 \times 10^{22} \dot{M}_{-7.5} \,\mathrm{g}$$
 (9)

or

$$\frac{M_h}{M_W} \approx 3 \times 10^{-3} \dot{M}_{-7.5}^{-1}.$$
 (10)

Thus, a leading part of the FRB heats a part of the wind to relativistic energies, which makes it more transparent to the trailing part of the emission. But the FRB energetics is not sufficient to make the wind fully transparent, so the estimates in Section 1.2 remain valid. Also, the momentum implanted by the FRB pulse, $P_{\text{FRB}} \sim E_{\text{FRB}}/c \sim 2 \times 10^{27} \, \text{g cm s}^{-1}$, is much smaller that the momentum of the wind within the orbital radius, $P_w \approx a\dot{M} = 7 \times 10^{30} \dot{M}_{-7.5} \, \text{g cm s}^{-1}$; the FRB pulse does not disturb the overall outflow. Moreover, the kinetic energy of the stellar wind $E_{w,\text{kin}} = M_w v_w^2/2 \approx 10^{39} \, \text{erg}$ is much larger compared to the FRB energy: $E_{\text{FRB}}/E_{w,\text{kin}} \sim 1/20$, so FRB impact on the flow dynamics can be neglected.

Nonlinear effects are strongly suppressed by the magnetic field (Lyutikov & Rafat 2019; Lyutikov 2020b). If the cyclotron frequency is larger than the wave frequency,

$$\omega_B \geqslant \omega \to B \geqslant 350\nu_9 \,\mathrm{G},$$
 (11)

then instead of large amplitude oscillations with p_{\perp} given by Equation (5) a particle experiences E×B drift. Magnetic fields of this order do occur in early-type stars (e.g., Petit et al. 2019).

2. Predictions: Mild DM Variations and Frequencydependent Activity Window

There is a number of predictions. As a simple educated guess, we predict variations of the dispersion measure (DM) within the observed window, and an increase of the activity window at higher frequencies. First we give simple order-of-magnitude estimates, and then demonstrate that the reality is likely to be more complicated. (RM and DM variations in wind of the binary pulsar PSR B1259 have been discussed by Kochanek 1993, Johnston et al. 1994, and Melatos et al. 1995.)

In a homogeneous wind a DM from a given point located distance a from the central star and propagating with angle ϕ with respect to the radial direction (ϕ is assumed to be fixed—we neglect possible plasma lensing effects) is

$$DM(\phi) = \int_{a}^{\infty} \frac{n_0 a^2}{x^2 + (x - a)^2 \tan^2 \phi} \frac{dx}{\cos \phi} = \frac{\phi}{\sin \phi} DM_0,$$
(12)

where

$$DM_0 \approx 0.8 \,\dot{M}_{-7.5} \eta_{a,1.5}^{-1} m_{\text{tot},1}^{-1/3} v_{w,8.5}^{-1} \tag{13}$$

is the dispersion measure for a radial ray. For larger ϕ the DM and the optical depth, see below, increase as the light ray passes longer distances at higher densities.

The wind can also produce rotation measure (RM) for the FRB pulse. To estimate the RM contribution of the wind, we

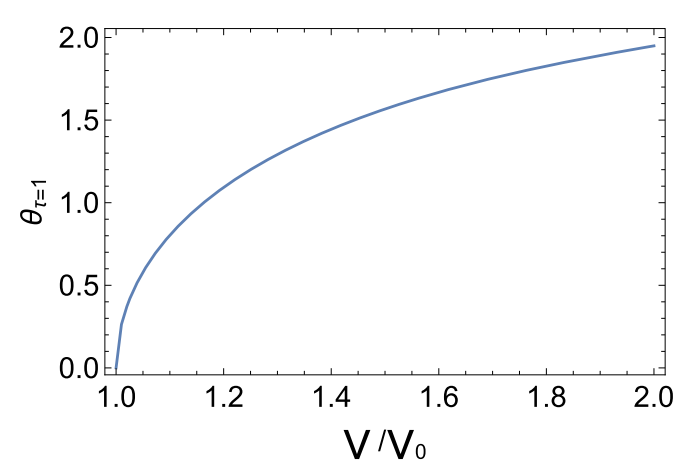


Figure 2. Dependence of the transparency angle ϕ on the observing frequency ν/ν_0 in idealized homogeneous wind. At the base frequency ν_0 the radial (outward-propagating) rays have $\tau=1$. At larger frequencies the rays at larger angles can escape; see also Figure 4.

scale the Alfvén velocity in the wind with the wind velocity, $v_A = \eta_A v_w$, where $\eta_A \sim 10^{-1}$. We find

$$RM = 7 \times 10^{3} (\phi \csc^{2} \phi - \cot \phi)$$
$$\times \eta_{A,-1} \eta_{a,1.5}^{-2} \dot{M}_{-7.5}^{3/2} v_{w,8.5}^{-1/2}. \tag{14}$$

The narrow transparency window, $\phi \ll 1$, will further reduce the RM as the radio signal propagates mostly orthogonally to the toroidal magnetic field in the wind (angular function in parentheses $\propto \phi/3$ for $\phi \to 0$).

Though the RM estimate (14) is fairly high, it is a sensitive function of the assumed parameters: the uncertainties in the magnetic field of the main-sequence star (Petit et al. 2019), wind dynamics (e.g., ratio of the wind's velocity to the Alfvén velocity in the wind), and the geometry of the magnetic field in the wind. Observationally, a large RM $\sim\!10^5\,\mathrm{rad}\,\mathrm{m}^{-2}$ was indeed observed in the case of FRB 121102 (Michilli et al. 2018), while FRB 180916.J0158+65 had a small RM $\sim\!144\,\mathrm{rad}\,\mathrm{m}^{-2}$ that may be completely due to the Galactic foreground interstellar medium (ISM; CHIME/FRB Collaboration et al. 2019). For the Sun the RM is $\sim\!10$ (Sakurai & Spangler 1994); we are not aware of RM measurements in the winds of massive stars.

Similarly, in a homogeneous wind an optical depth to a given point (assuming isothermal wind) is

$$\tau(\phi) \propto \int_{a}^{\infty} \left(\frac{n_0 a^2}{x^2 + (x - a)^2 \tan^2 \phi}\right)^2 \frac{dx}{\cos \phi}$$

$$\tau(\phi) = \frac{3}{2} (\phi \csc^3(\phi) - \cot(\phi) \csc(\phi)) \tau_0, \tag{15}$$

where $\tau_0 = \tau(\phi=0)$. The optical depth for radial propagation depends on frequency, Equation (3):

$$\tau_0 \propto \nu^{-2.1}$$
. (16)

Let ν_0 be the frequency such that $\tau_0(\nu_0=1)$. At higher frequencies an optical depth of 1 is reached at the angles pictured in Figure 2.

The above estimates assume idealized smooth wind. As numerical simulations demonstrate, Figure 1, the plasma around the bow shock is highly inhomogeneous. The pulsar wind creates a tail cavity and an accumulation of dense material around the head. This plasma "wall" will have an especially

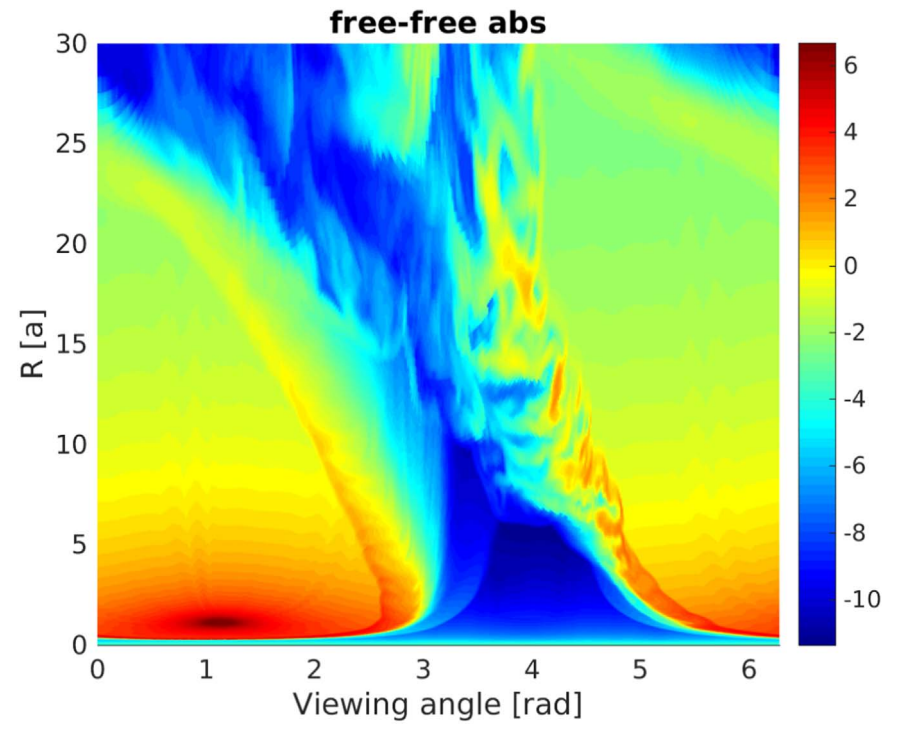


Figure 3. Profiles of the differential absorption optical depth (color, depends on viewing angle and distance from compact object R) along different lines of sight calculated near the apastron orbital phase (see details in Bosch-Ramon et al. 2015). Low values (blue color) correspond to the transparency window.

large effect on the free-free absorption (see Figure 3), since it depends on density squared. A plasma wall can be opaque to a broad range of frequencies, erasing a simple correlation between the active window and the observing frequency.

We also calculated dispersion measure and free-free absorption using the three-dimensional relativistic hydrodynamical simulation by Bosch-Ramon et al. (2015) of the interaction of a massive stellar wind with the pulsar wind. In their setup, the pulsar is moving on an elliptic orbit with eccentricity e = 0.24 and orbital period 3.4 days. We reprocessed the data for the orbital period of 16 days. (Eccentricity for high-mass binaries with a compact object and orbital period of about 15 days can vary from 0 until 0.85; Townsend et al. 2011; Tauris et al. 2017.) In Figure 4, we show the profiles of the integrated density, $\int n \propto DM$, and integrated density squared, $\int n^2 \propto \tau$ (the absorption optical depth), along different lines of sight. Figure 4 demonstrates that at each moment there is a narrow transparency window with a duration from ~ 0.1 (close to apastron) to ~ 0.3 (close to periastron) orbital periods. Note that a wide transparency window can be affected by the turbulent motion and can be chaotically transparent and opaque from orbit to orbit.

Our analysis demonstrates that the DM and free-free absorption show high correlation. The transparent window corresponds to a minimum DM: this can explain the small change of DM for repeating FRBs. On the other hand, the variations of the DM within the transparency window are smaller by a factor of a few than the overall variations, Figure 4.

In addition, simulations show a sharp rise and decay in transparency near the periastron phase, while in the direction of apastron such variations are more gradual, Figure 4 (bottom panel). Thus, we expect/predict orbital-dependent spectral evolution: bursts near borders of the transparency window

could be bluer. Observational confirmation of such an effect can be a smoking gun for our model.

3. Discussion

In this Letter we discuss a model for the periodicity observed in FRB 180916.J0158+65 by the CHIME telescope (The CHIME/FRB Collaboration et al. 2020). The working model is that the FRBs are produced by a neutron star that orbits an OB primary. The periodicity arises due to free-free absorption in the primary's (of the massive star's) wind. Thus, we argue that the observed periodicity is a property of a particular system and is likely not essential for the FRB production. On the other hand, the association of an FRB with a compact stellar binary further strengthens the magnetospheric loci of FRBs, as argued by Popov & Postnov (2013), Lyutikov et al. (2016), Lyutikov (2020a), and Lyutikov & Rafat (2019) also see reviews by Cordes & Chatterjee (2019) and Petroff et al. (2019). Note that FRB 180916.J0158+65 also shows narrow emission bands drifting down in frequency—this is naturally interpreted as a plasma laser operating in a neutron star's magnetosphere and showing radius-to-frequency mapping (Lyutikov 2020a).

Observations of FRB 121102 by Rajwade et al. (2020) indicated periodicity of $P \sim 160$. We identify this periodicity with the orbital motion. The present model is applicable to the case of FRB 121102 as well. Following Equation (3) we can estimate the maximal orbital separation to absorb the radio signal, 2×10^{13} cm. This would correspond to the orbital period ~ 200 days.

Most importantly, both FRB 180916.J0158+65 (The CHIME/FRB Collaboration et al. 2020) and FRB 121102 (Bassa et al. 2017; Chatterjee et al. 2017; Tendulkar et al. 2017) are observed in star-forming regions. This is consistent with the OB primary.

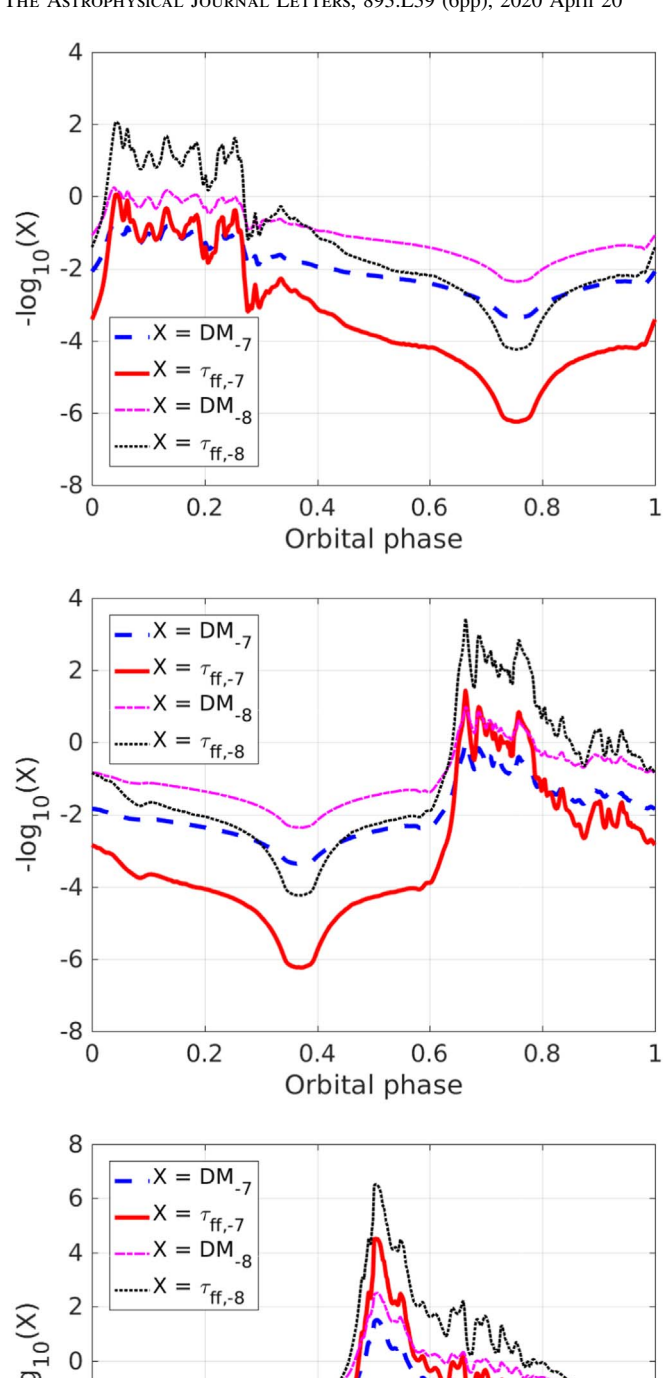


Figure 4. Profiles of the DM (dashed blue: $\dot{M}_w = 10^{-7} M_{\odot} \, \mathrm{yr}^{-1}$ and dotted-dashed magenta: $\dot{M}_w = 10^{-8} M_{\odot} \, \mathrm{yr}^{-1}$) and absorption optical depth (solid red: $\dot{M}_w = 10^{-7} M_{\odot} \, \mathrm{yr}^{-1}$ and dotted black: $\dot{M}_w = 10^{-8} M_{\odot} \, \mathrm{yr}^{-1}$) depending on orbital phases calculated at three different lines of sight in the equatorial plane (close to apastron—top, intermediate phase—center, and close to periastron—bottom). Here we use the same hydrodynamical model as in Figure 3, the orbital eccentricity e=0.24. Large values of $-\log \tau$ (red curves) correspond to the transparency window.

Orbital phase

0.4

0.6

8.0

-2

-4

-6

-8

0

0.2

The model has three clear predictions: (i) mild variations of DM, Equation (13), should be observed in the activity window; (ii) the activity window should be broader at higher frequencies, Figure 2; (iii) large RM should be measured in FRB 180916.J0158+65 2. Importantly, in our model the binarity is not an intrinsic property of FRBs: FRB 121102 and FRB 180916.J0158+65 happen to be in binaries, other FRB sources can be isolated: in that case no large RMs are expected.

Interestingly, a new, unusual radiative mechanism operates when an FRB pulse enters the primary's wind: heating of a narrow layer of plasma to relativistic energies by a radio beam. We are not aware of such processes in any other astrophysical system. Corresponding bursts of X-ray emission are likely to be too weak to be observable.

We constrain the primary to be a late O-type/early B-type star: earlier types have too powerful winds that remain heavily optically thick at the inferred orbital separation, while later types produce winds that are too weak—this runs contrary our interpretation of the small orbital activity window as a pointing to the momentum dominance of the primary's wind over the pulsar's. Since the primary's momentum loss should overpower the pulsar's wind—the pulsar can be only mildly strong, with a spin-down luminosity $L_{\rm sd} \sim 10^{37} \ {\rm erg \ s^{-1}}$; this value is somewhat larger than the spin-down power of Galactic magnetars.

Periodic transparency can also be achieved by having a highly eccentric orbit—then at an apastron the radio pulses would sample lower-density plasma. We disfavor this scenario since it predicts a large active window (since the binary would spend more time at large separations).

Sharp boundaries of the wind cavity can also lead to refractive effects. For isotropic FRBs, the reflection from the walls of the wind cavity will redistribute radio impulse in time so that its luminosity will be suppressed by a factor $4\pi T_{\rm FRB} c/\Omega_{\rm cone} a\eta \sim 10^{-5}$. This will make it difficult to detect the reflected signal. On the other hand, if FRBs have a narrow cone structure, then we could possibly see several echoes formed by turbulence on cavity walls.

The present model has a number of similarities to binary systems containing pulsars. First, binary pulsars PSR 1957+20 and PSR 1744-24A show periodic orbital-dependent eclipses (limited to \sim 10% in phase in the case of PSR 1957+20 and \sim 50% in the case of PSR 1744-24A; Rasio et al. 1989, 1991; Lyne et al. 1990). These are low-mass binaries, ablated by the NS's wind (Phinney et al. 1988), so the wind–wind interaction is dominated by the pulsar's wind, $\eta \geqslant 1$. In that case a number of plasma effects, like variations of the DM and pulse delays, do show during the eclipse. Then, there is a number of γ -ray binaries that contain (or are thought to contain) neutron stars (Dubus 2013; Barkov & Bosch-Ramon 2016, 2018; Bosch-Ramon et al. 2017; Abeysekara et al. 2018)

In our view, the observed periodicity in FRB 180916.J0158 +65 does fit with a general concept of neutron stars' magnetospheres being the *loci* of FRBs. Identification of FBRs with neutron stars leaves two possibilities for the energy source: rotational (akin to Crab's giant pulses; Popov et al. 2006; Lyutikov 2007; Mickaliger et al. 2012; Lyutikov et al. 2016) or magnetar-like magnetically powered emission (Eichler et al. 2002; Lyutikov 2002). The present model confirms that FRBs are not rotationally powered (since the present model requires that the pulsar wind should be mild/weak; Lyutikov 2017). The magnetically powered model, radio emission

1

generated in the magnetospheres of neutron stars, remains the most probable, in our view.

Finally, can the FRBs' radio emission be induced by the interactions of the companions? Clearly not. The orbital motionally induced electric potential potential and luminosity for scaling (A1) estimate to

$$\Phi_{\text{orb}} = eBa\beta_{\text{orb}} = 2 \times 10^{13} b_q \text{ eV}$$

$$L_{\text{orb}} \sim (\Phi_{\text{orb}}/e)^2 c = 2 \times 10^{31} b_q^2 \text{ erg s}^{-1}, \tag{17}$$

where we scaled the surface magnetic field to a quantum field, $b_q = B_{\rm NS}/B_Q$, $B_Q = m_e^2 c^3/(e\hbar)$. Estimates (17) give very weak power, even for quantum-strong magnetic fields, and small potential. We conclude that even in the tightest orbit case of geodetically induced precession, the powers expected due to the interaction of the binaries are very small (Lyutikov 2004; Lyutikov & Thompson 2005; Lomiashvili & Lyutikov 2014). (Note that binary pulsar PSR0737B, which shows strong magnetospheric interaction, is/was an exceptionally weak pulsar—it cannot not be used as a model for FRBs, the most powerful radio emitters.) Hence, we conclude that binarity is not a cause of FRB emission.

M.L. would like to acknowledge support by NASA grant 80NSSC17K0757 and NSF grants 10001562 and 10001521. We would like to thank Jason Hessels, Victoria Kaspi, Jonathan Katz, Wenbin Lu, and Elizaveta Ryspaeva for discussions and Yegor Lyutikov for help with the illustration.

Appendix Unlikely Alternative: FRB Variations due to Geodetic Precession

Another possible source of variability is a the geodetic precession that makes the active region periodically aligned with the line of sight. For example, in the binary pulsar PSR 0737 the geodetic precession led to the disappearance of the PSR 0737B (Breton et al. 2008; Lomiashvili & Lyutikov 2014). To have a geodetic precession of only 16 days the required orbital size is

$$\Omega_G = \left(\frac{2\pi}{P}\right)^{5/3} \left(\frac{GM_{\odot}}{c^3}\right)^{5/3} \left(\frac{m_{\rm MS}(4m_{\rm PSR} + 3m_{\rm MS})}{2(m_{\rm PSR} + m_{\rm MS})^{4/3}}\right)
a = 2 \times 10^9 \frac{(m_{\rm MS}(4m_{\rm PSR} + 3m_{\rm MS})^{2/5}}{(m_{\rm PSR} + m_{\rm MS})^{1/5}} \text{ cm.}$$
(A1)

Gravitational decay time is still sufficiently long,

$$t_{\rm GW} = 670 \frac{m_{\rm MS}^{2/5}}{m_{\rm DCD}} \, \text{yr}$$
 (A2)

(where $m_{\rm MS} \geqslant m_{\rm PSR}$ was assumed).

The system with a separation of (A1) will be exceptional. Strong modifications of the magnetospheric properties may be expected in this case. For example, setting separation equal to the light cylinder, the period would be 0.75 s. Strong wind—magnetosphere interactions are expected, similar to the case of the binary pulsar PSR 0737A/B (Lyutikov 2004; Lyutikov & Thompson 2005; Lomiashvili & Lyutikov 2014).

ORCID iDs

Maxim Lyutikov https://orcid.org/0000-0001-6436-8304 Maxim V. Barkov https://orcid.org/0000-0002-0960-5407

References

```
Abeysekara, A. U., Benbow, W., Bird, R., et al. 2018, ApJL, 867, L19
Akhiezer, A. I., Akhiezer, I. A., Polovin, R. V., Sitenko, A. G., &
   Stepanov, K. N. 1975, Plasma electrodynamics. Volume 1 - Linear
   theory. Volume 2 - Non-linear theory and fluctuations (Oxford: Pergamon
Barkov, M. V., & Bosch-Ramon, V. 2016, MNRAS, 456, L64
Barkov, M. V., & Bosch-Ramon, V. 2018, MNRAS, 479, 1320
Bassa, C. G., Tendulkar, S. P., Adams, E. A. K., et al. 2017, ApJL, 843, L8
Bosch-Ramon, V., & Barkov, M. V. 2011, A&A, 535, A20
Bosch-Ramon, V., Barkov, M. V., Khangulyan, D., & Perucho, M. 2012,
   A&A, 544, A59
Bosch-Ramon, V., Barkov, M. V., Mignone, A., & Bordas, P. 2017, MNRAS,
  471, L150
Bosch-Ramon, V., Barkov, M. V., & Perucho, M. 2015, A&A, 577, A89
Breton, R. P., Kaspi, V. M., Kramer, M., et al. 2008, Sci, 321, 104
Chatterjee, S., Law, C. J., Wharton, R. S., et al. 2017, Natur, 541, 58
CHIME/FRB Collaboration, Andersen, B. C., Bandura, K., et al. 2019, ApJL,
   885, L24
Cordes, J. M., & Chatterjee, S. 2019, ARA&A, 57, 417
Dubus, G. 2013, A&ARv, 21, 64
Eichler, D., Gedalin, M., & Lyubarsky, Y. 2002, ApJL, 578, L121
Fruchter, A. S., Stinebring, D. R., & Taylor, J. H. 1988, Natur, 333, 237
Johnston, S., Manchester, R. N., Lyne, A. G., Nicastro, L., & Spyromilio, J.
   1994, MNRAS, 268, 430
Kochanek, C. S. 1993, ApJ, 406, 638
Krticka, J. 2014, A&A, 564, A70
Lang, K. R. 1999, Astrophysical Formulae (New York: Springer)
Levin, Y., Beloborodov, A. M., & Bransgrove, A. 2020, arXiv:2002.04595
Lomiashvili, D., & Lyutikov, M. 2014, MNRAS, 441, 690
Lu, W., & Phinney, E. S. 2019, arXiv:1912.12241
Lyne, A. G., Manchester, R. N., D'Amico, N., et al. 1990, Natur, 347, 650
Lyutikov, M. 2002, ApJL, 580, L65
Lyutikov, M. 2004, MNRAS, 353, 1095
Lyutikov, M. 2007, MNRAS, 381, 1190
Lyutikov, M. 2017, ApJL, 838, L13
Lyutikov, M., & Rafat, M. 2019, arXiv:1901.03260
Lyutikov, M. 2020a, ApJ, 889, 135
Lyutikov, M. 2020b, arXiv:2001.09210
Lyutikov, M., Burzawa, L., & Popov, S. B. 2016, MNRAS, 462, 941
Lyutikov, M., & Thompson, C. 2005, ApJ, 634, 1223
Melatos, A., Johnston, S., & Melrose, D. B. 1995, MNRAS, 275, 381
Michilli, D., Seymour, A., Hessels, J. W. T., et al. 2018, Natur, 553, 182
Mickaliger, M. B., McLaughlin, M. A., Lorimer, D. R., et al. 2012, ApJ,
Petit, V., Wade, G. A., Schneider, F. R. N., et al. 2019, MNRAS, 489, 5669
Petroff, E., Hessels, J. W. T., & Lorimer, D. R. 2019, A&ARv, 27, 4
Phinney, E. S., Evans, C. R., Blandford, R. D., & Kulkarni, S. R. 1988, Natur,
Popov, M. V., Soglasnov, V. A., Kondrat'Ev, V. I., et al. 2006, ARep, 50, 55
Popov, S. B., & Postnov, K. A. 2013, arXiv:1307.4924
Rajwade, K. M., Mickaliger, M. B., Stappers, B. W., et al. 2020, arXiv:2003.
  03596
Rasio, F. A., Shapiro, S. L., & Teukolsky, S. A. 1989, ApJ, 342, 934
Rasio, F. A., Shapiro, S. L., & Teukolsky, S. A. 1991, A&A, 241, L25
Sakurai, T., & Spangler, S. R. 1994, ApJ, 434, 773
Tauris, T. M., Kramer, M., Freire, P. C. C., et al. 2017, ApJ, 846, 170
Tendulkar, S. P., Bassa, C. G., Cordes, J. M., et al. 2017, ApJL, 834, L7
The CHIME/FRB Collaboration, Amiri, M., Andersen, B. C., et al. 2020,
  arXiv:2001.10275
Townsend, L. J., Coe, M. J., Corbet, R. H. D., & Hill, A. B. 2011, MNRAS,
  416, 1556
Vink, J. S., de Koter, A., & Lamers, H. J. G. L. M. 2001, A&A, 369, 574
Zanazzi, J. J., & Lai, D. 2020, ApJL, 892, L15
```